Chemical Engineering Science 82 (2012) 104–113

Contents lists available at SciVerse ScienceDirect

Chemical Engineering Science

journal homepage: www.elsevier.com/locate/ces

MP-PIC simulation of CFB riser with EMMS-based drag model

Fei Li [a,*], Feifei Song [a], Sofiane Benyahia [b], Wei Wang [a], Jinghai Li [a]

[a] State Key Laboratory of Multi-phase Complex Systems, Institute of Process Engineering, Chinese Academy of Sciences, Beijing 100190, China
[b] National Energy Technology Laboratory, Morgantown, WV 26507, USA

HIGHLIGHTS

- Combination of the MP-PIC method with the EMMS drag force model.
- Dense flows in CFB risers were accurately simulated with this method.
- We examine the effects of the number of particles per parcel (n_p) on simulations.
- There exists a critical n_p, below which, the stable solid flux can be achieved.
- Below another critical n_p, decreasing n_p will increases the simulation time.

ARTICLE INFO

Article history:
Received 31 December 2011
Received in revised form
7 June 2012
Accepted 13 July 2012
Available online 27 July 2012

Keywords:
MP-PIC
EMMS
Drag model
Riser
Simulation
Fluidization

ABSTRACT

MP-PIC (multi-phase particle in cell) method combined with the EMMS (energy minimization multi-scale) drag force model was implemented with the open source program MFIX to simulate the gas–solid flows in CFB (circulating fluidized bed) risers. Calculated solid flux by the EMMS drag agrees well with the experimental value; while the traditional homogeneous drag over-predicts this value. EMMS drag force model can also predict the macro- and meso-scale structures. Quantitative comparison of the results by the EMMS drag force model and the experimental measurements show high accuracy of the model. The effects of the number of particles per parcel and wall conditions on the simulation results have also been investigated in the paper. This work proved that MP-PIC combined with the EMMS drag model can successfully simulate the fluidized flows in CFB risers and it serves as a candidate to realize real-time simulation of industrial processes in the future.

1. Introduction

Numerical simulation is a powerful tool in the investigation of fluidization engineering, which can aid in the optimization of design and operation of the real processes. Reports show that virtual experiments that are full-loop simulation of industrial scale reactors can be achieved using large scale parallel computing (Zhang et al., 2008, 2010). However, tens of hours are needed to simulate even one second real process, which is far from the demand of rapid simulation or even the real-time simulation. Recently, the rapid development in computer hardware, specifically the graphic process unit (GPU) which can efficiently handle the parallel computing of independent data, has promoted the dream of rapid simulation of real processes come true (Ge et al., 2011). For fluidization engineering, rapid simulation requires not only efficient but also accurate simulation of fluidization phenomenon in fluidized beds. In our group, a EMMS based drag force model was developed and this model has been coupled with the two-fluid model (TFM) to successfully simulate the gas–solid flow field in risers (Yang et al., 2003; Wang and Li, 2007; Wang et al., 2008a,b; Li, 2009; Lu, 2009). Reported results show that simulation with the EMMS based drag force model can give a much higher accuracy than simulation with the traditional homogeneous drag force model (Jiradilok et al., 2006; Qi et al., 2007; Nikolopoulos et al., 2010; Benyahia, 2011; Lu et al., 2011). So the EMMS based drag force model fulfills the accuracy requirement for rapid simulation. As mentioned above, the development of high performance computing in recent years has provided the hardware foundation for rapid simulation. Specifically, a large computer system (mole-8.5) with hybrid computing structure which consists of CPU and GPU and reaches Petaflops range is available in our group (Chen et al., 2009; Ge et al., 2011). Finally, a proper computing method is required to fulfill efficiency demand to realize rapid simulation.

* Corresponding author. Tel.: +86 10 82544843; fax: +86 10 62558065.
E-mail address: lifei@home.ipe.ac.cn (F. Li).

0009-2509/$ - see front matter © 2012 Elsevier Ltd. All rights reserved.
http://dx.doi.org/10.1016/j.ces.2012.07.020

There are three main suitable computing methods for the dense gas–solid fluidization, including two-fluid model (TFM) simulation (Ishii, 1975; Gidaspow, 1994; Neri and Gidaspow, 2000), discrete element method (DEM) (Tsuji et al., 1992, 1993; Deen et al., 2007; Chu and Yu, 2008) and multi-phase particle-in-cell (MP-PIC) method (Andrews and O'Rourke, 1996; Snider, 2001; Benyahia and Galvin, 2010; Pirker et al., 2010).

For TFM method, particle phase is assumed to be a pseudo fluid and the two phases interpenetrating with each other. Partial differential equations describing the two-phase hydrodynamics are always discretized to form linear equations and variables of neighbor cells are interrelated, thus these equations are not suitable to be solved with CPU–GPU hybrid computing. On the other hand, when the number of solid phase increases that is to say with poly-dispersed particles, the equation set becomes very large and the computing load will increase dramatically.

For DEM, particles are treated as real spheres with different diameters, and particle interaction is treated as particle collision. Thus, particles are interrelated with each other, which is also not suitable for CPU–GPU hybrid computing.

For MP-PIC method, particles are treated as parcels and each parcel contains a certain number of real particles of the same diameter (Snider, 2001). The particle interaction is considered through the solid phase normal stress but not directly through particle collision, thus particles move independently from the view of numerical computing whose computation speed can be remarkably accelerated on CPU–GPU hybrid computing platform (Xiong et al., 2010). In addition, MP-PIC method needs not to take the particle collisions implicitly, hence a much bigger time step can be adopted, specifically the time step for particle calculation is the same with that for fluid calculation, which can further accelerate the calculation. In MP-PIC method, it is the "parcel" that has to be tracked but not the real particle, which can also reduce the computing effort greatly. All these advantages make MP-PIC simulation of the large scale particle fluidization system much faster. And with this calculation mode, it is expected to satisfy the efficiency demand of rapid simulation.

Other coarse grained simulation methods have also been reported, just like the similar-particle-assembly (SPA) model (Kuwagi et al., 2004; Mokhtar et al., 2011), DEM simulation based on particle cluster (Liu et al., 2006) and so on. Generally, those methods assume a representative particle with much larger diameter instead of original fine particle and the soft sphere model is used to describe particle collision. However, a criterion to determine the representative particle diameter is still absent as well as the collision parameters.

Since the homogeneous drag force model used in the present MP-PIC method is inaccurate when simulating complex flows with coarse mesh, and as a first step to realize rapid simulation, the primary goal of this study is to integrate MP-PIC and the EMMS based drag force model with the open source multi-phase simulation program MFIX (Syamlal et al., 1993). Subsequently, the gas–solid flow in a CFB riser is simulated to verify the accuracy of the EMMS modified MP-PIC method. Finally, the effects of different model parameters, including the parcel–wall interaction conditions and the number of particles per parcel are investigated.

2. Numerical models and simulation settings

2.1. MP-PIC method

MP-PIC method was first developed by Andrews and O'Rourke to simulate dense particulate flows (1996). In this method, the gas phase is described with the Eulerian type equations which are very similar to the equations in the TFM method. While for the solid phase, a certain number of particles with the same diameter and velocity are represented by a parcel, and the parcels are tracked with the Newton's Law. Particles do not collide with each other, but take effect through solid phase normal stress (Patankar and Joseph, 2001; Snider, 2001; Benyahia and Galvin, 2010). In practice, all the parcels in a fluid cell are responsible for the solid phase normal stress on the cell grid. The solid phase normal stress is first calculated on the fluid grid point, and then it is interpolated to the parcel location. The governing equations of the MP-PIC method are as follows (Snider, 2001):

Gas phase continuity equations:

$$\frac{\partial}{\partial t}(\varepsilon_g\rho_g)+\nabla\cdot(\varepsilon_g\rho_g\vec{u}_g)=0 \tag{1}$$

where the subscript g represents the gas phase.

Gas phase momentum equations:

$$\frac{\partial}{\partial t}(\varepsilon_g\rho_g\vec{u}_g)+\nabla\cdot(\varepsilon_g\rho_g\vec{u}_g\vec{u}_g)=-\varepsilon_g\nabla p+\nabla\cdot\bar{\bar{\tau}}_g+\varepsilon_g\rho_g\vec{g}-\sum_{p=1}^{n_T}n_p\frac{V_p}{V_c}\beta_p(\vec{U}_g(\vec{x}_p)-\vec{U}_p) \tag{2}$$

where n_T is the parcel number in the fluid cell and n_p is the number of particles per parcel. V_p and V_c are the volumes of particle and fluid cell, respectively. β_p is the drag force coefficient, $\vec{U}_g(\vec{x}_p)$ is the gas velocity at parcel location, $\vec{x}_p$, and $\vec{U}_p$ is the parcel velocity. $\bar{\bar{\tau}}_g$ is the gas phase stress tensor

$$\bar{\bar{\tau}}_g=2\mu_g\bar{\bar{S}}_g,\quad \bar{\bar{S}}_g=\frac{1}{2}\left[\nabla\vec{u}_g+(\nabla\vec{u}_g)^T\right]-\frac{1}{3}\nabla\cdot\vec{u}_g\bar{\bar{I}} \tag{3}$$

Parcel motion equations:

$$\frac{d\vec{x}_p}{dt}=\vec{U}_p \tag{4}$$

$$\frac{d\vec{U}_p}{dt}=-\frac{\nabla p}{\rho_s}-\frac{\nabla p_s}{\varepsilon_s\rho_s}+\vec{g}+\frac{\beta_p}{\rho_s}(\vec{U}_g(\vec{x}_p)-\vec{U}_p) \tag{5}$$

where p_s is the particle pressure, which can be expressed as (Snider, 2001; Benyahia and Sundaresan, 2011)

$$p_s=\frac{P_s^*\varepsilon_s^\alpha}{\varepsilon_{s,\max}-\varepsilon_s} \tag{6}$$

where P_s^*, α, are model parameters, $\varepsilon_{s,\max}$ is the solid volume fraction at close pack. Their values are summarized in Table 1.

2.2. Drag force model

Drag force modeling is of great importance to accurately simulate the solid distribution in CFB risers with two-fluid model. Most recently, Benyahia and Sundaresan also indicated that homogeneous drag force model is insufficient to capture complex gas–solid flow structures with discrete particle models when using coarse mesh (Benyahia and Sundaresan, 2011). Here, homogeneous drag model describes the drag force exerted on particles which are homogeneously distributed in gas flows. Particles in CFB risers usually aggregate to form clusters, which lead to local heterogeneous solid distributions. Specifically, particle cluster diameter has been found to be a function of a lots parameters, including particle diameter, gas and solid velocities, etc. (Li and Kwauk, 1994; Breault, 2012). EMMS theory does not describe clusters directly, but it uses flow field decomposition and energy minimization to characterize local heterogeneous solid distributions. Then the decomposed field parameters are used to formulate the EMMS drag (Wang and Li, 2007). In this study, a traditional homogeneous drag force model (Ergun, 1952;

Table 1
Parameters used in the EMMS based drag force model (Lu, 2009; Lu et al., 2011).

Quantity	Riser 1	Riser 2
Riser diameter, D (m)	0.05	0.09
Riser height, H (m)	2.79	10.5
Operating temperature, T_{op} (K)	297	298
Operating pressure, P_{op} (Pa)	1.01×10^5	1.01×10^5
Particle diameter, d_p (μm)	60	54
Particle density, ρ_s (kg/m^3)	1000	930
Gas density, ρ_g (kg/m^3)		Calculated using ideal gas law (about 1.2)
Gas viscosity, μ_g (Pa s)	1.8×10^{-5}	1.9×10^{-5}
Superficial gas velocity, U_{g0} (m/s)	1.17	1.52
Solids flux, G_s (kg/(m^2 s))		Calculated
Initial average solid volume fractions, $\varepsilon_{s,ini}$	0.086	0.106
Solid volume fraction at close pack, $\varepsilon_{s,max}$		0.6
Particle pressure parameter, P_s^* (Pa)		100
Particle pressure parameter, α		2
Particle–wall restitution coefficient, e_w	0.9, 0.99	0.9
Number of particles per parcel, n_p	10, 20, 50, 100, 200, 500, 1000, 2000, 4000, 8000, 160,000	500, 1000
Number of cells, $I\times J$	60×80, 10×100, 20×100, 20×150, 20×200, 30×300, 40×300	40×225, 20×225
Time step, Δt (s)		Variable (10^{-6}–10^{-3})
Simulation time, t (s)	20	25

Wen and Yu, 1966) and the EMMS based drag force model (Lu, 2009; Lu et al., 2011) are used and compared.

Homogeneous drag force model:

$$\beta_p=\begin{cases}150\frac{\mu_g\varepsilon_s}{\varepsilon_g d_p^2}+1.75\frac{\rho_g|\vec{U}_g(\vec{x}_p)-\vec{U}_p|}{d_p}, & \varepsilon_g<0.8\\ \frac{3}{4}\frac{\varepsilon_g\rho_g|\vec{U}_g(\vec{x}_p)-\vec{U}_p|}{d_p}C_{D0}\varepsilon_g^{-2.7}, & \varepsilon_g\geq0.8\end{cases}\tag{7}$$

$$C_{D0}=\begin{cases}\frac{24(1+0.15Re_p^{0.687})}{Re_p}, & Re_p<1000\\ 0.44, & Re_p\geq1000\end{cases},\quad Re_p=\frac{\varepsilon_g\rho_g|\vec{U}_g(\vec{x}_p)-\vec{U}_p|d_p}{\mu_g}\tag{8}$$

EMMS based drag force model:

$$\beta_p=\frac{3}{4}\frac{\varepsilon_g\rho_g|\vec{U}_g(\vec{x}_p)-\vec{U}_p|}{d_p}C_{D0}\varepsilon_g^{-2.7}H_D\tag{9}$$

$$H_D=a(Re_p+b)^c\tag{10}$$

where H_D is the heterogeneity index, and a, b, and c are the model parameters as listed in Table 2.

2.3. Wall treatment for parcels

A bounce-back condition was used for parcel–wall collisions (Galimov et al., 2005), that is

$$\vec{n}\cdot\vec{U}_p=-e_w\vec{n}\cdot\vec{U}_p^{(0)}\tag{11}$$

$$\vec{t}\cdot\vec{U}_p=e_w\vec{t}\cdot\vec{U}_p^{(0)}\tag{12}$$

where e_w is the restitution coefficient for particle–wall collision, $\vec{n}$ and $\vec{t}$ are the unit, normal and tangential vectors of wall, respectively, and $\vec{U}_p^{(0)}$ is the parcel velocity before collision with wall.

2.4. Simulation conditions

The CFB experiments reported by Horio et al.(1988) and Li and Kwauk (1994) were adopted here to be the test cases. Only the risers were simulated. Horio's riser with 2.79 m in height and 0.05 m in diameter was denoted as riser 1 and Li and Kwauk's riser with 10.5 m in height and 0.09 m in diameter is denoted as riser 2. Fig. 1a and b shows the experimental CFB schemes. The simplified 2D calculation domain is shown in Fig. 1c, where

Table 2
Parameters for simulations.

$\begin{cases}a=0.8526-\frac{0.5846}{1+(\varepsilon_g/0.4325)^{22.6279}}\\ c=0\end{cases}$	$0.4\leq\varepsilon_g<0.46$
$\begin{cases}a=0.0320+\frac{0.7399}{1+(\varepsilon_g/0.4912)^{54.4265}}\\ b=0.00225+\frac{772.0074}{1+10^{66.3224(\varepsilon_g-0.3987)}}+\frac{0.02404}{1+10^{53.8948(0.5257-\varepsilon_g)}}\\ c=0.1705-\frac{0.1731}{1+(\varepsilon_g/0.5020)^{37.7091}}\end{cases}$	$0.46\leq\varepsilon_g<0.545$
$\begin{cases}a=(2124.956-2142.3\varepsilon_g)^{-0.4896}\\ b=(0.8223-0.1293\varepsilon_g)^{13.0310}\\ c=\frac{(\varepsilon_g-1.0013)}{-0.06633+9.1391(\varepsilon_g-1.0013)+6.9231(\varepsilon_g-1.0013)^2}\end{cases}$	$0.545\leq\varepsilon_g<0.99$
$\begin{cases}a=0.4243+\frac{0.8800}{1+\exp(-(\varepsilon_g-0.9942)/0.00218)}\left(1-\frac{1}{1+\exp(-(\varepsilon_g-0.9989)/0.00003)}\right)\\ b=0.01661+0.2436\exp\left(-0.5\left(\frac{\varepsilon_g-0.9985}{0.00191}\right)^2\right)\\ c=0.0825-0.0574\exp\left(-0.5\left(\frac{\varepsilon_g-0.9979}{0.00703}\right)^2\right)\end{cases}$	$0.99\leq\varepsilon_g<0.9997$
$a=1$, $c=0$	$0.9997\leq\varepsilon_g\leq1$

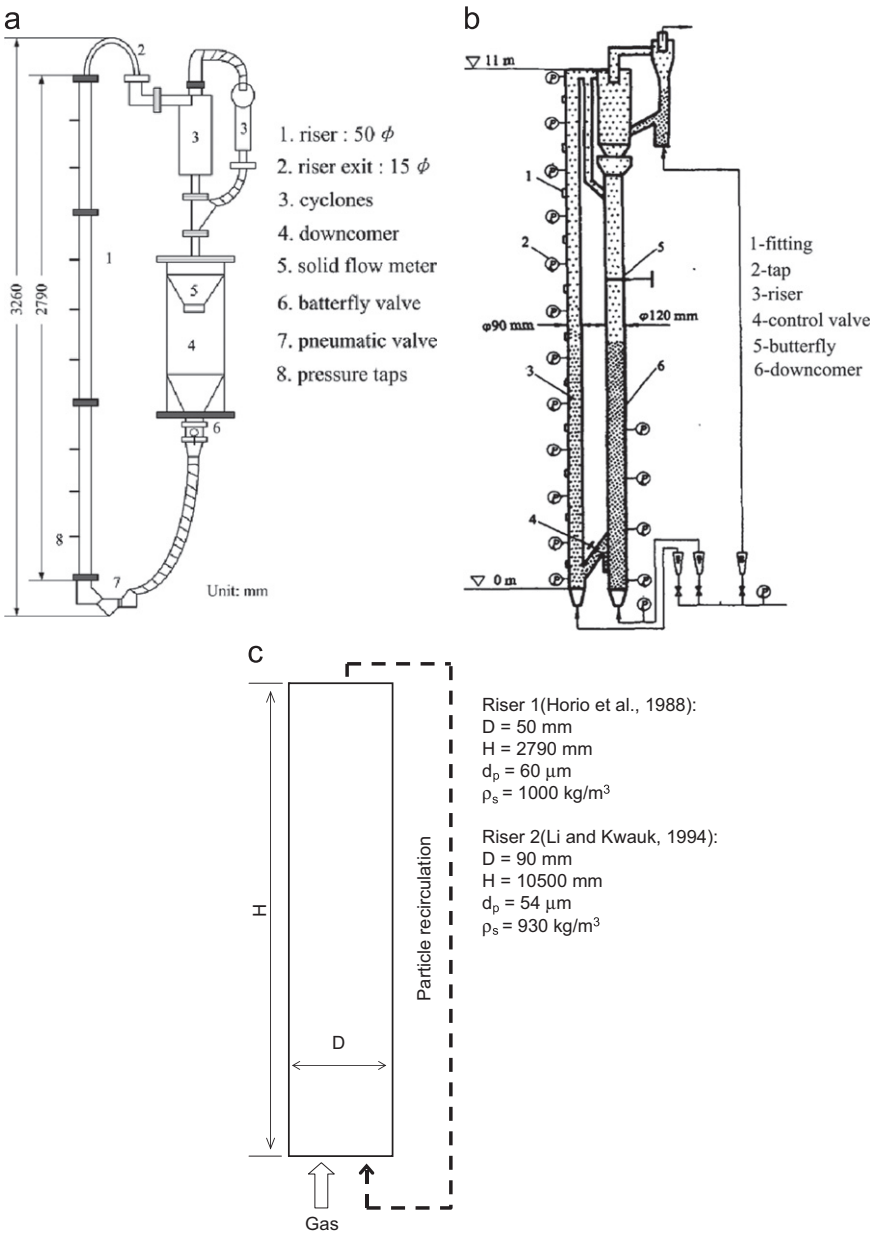

Fig. 1. Experimental CFB schemes and simplified 2D geometry of the risers: (a) experimental CFB scheme used by Horio et al.(1988); (b) experimental CFB scheme used by Li and Kwauk(1994); and (c) 2D geometry model of the risers, where D is the riser diameter and H is the riser height.

ambient air enters the riser from the bottom inlet and fluidizes FCC particles upward for the both risers. Both gas and particle flows out of the domain from the top pressure outlet, and the escaping particles are directly sent back to the riser from the bottom inlet to maintain the bed inventory constant. For riser 1, a grid test has been made as shown in Section 3.1, and finally 10×100 Cartesian grid was adopted in the subsequent simulations. While for riser 2, an optimal 40×225 Cartesian grid was adopted in this study according to Lu's two-fluid model simulations (Lu, 2009; Lu et al., 2011). For both risers, variable time step ranging from 10^{-6} to 10^{-3} s was used to aid convergence of the program. For riser 1, the cases lasted for 20 s. For riser 2, the cases last for 25 s, of which the initial 5 s were simulated with a much smaller inlet velocity, 0.5 m/s and after that, the inlet velocity was changed to maintain the bed superficial velocity of 1.52 m/s as listed in Table 1. For all the cases, the last 10 s were used for statistical analysis.

The other simulation conditions including gas and particle properties, operating conditions and particle pressure model parameters are listed in Table 1.

3. Results and analysis

3.1. Grid test for riser 1 with EMMS drag

Grid check has been conducted for riser 1. Fig. 2 shows that when using different grid numbers, calculated solid flux with EMMS drag force model are nearly constant which is also very close to the experimental value.

Fig. 3 further compares the axial voidage distribution calculated under different grid resolutions. The figure shows that except for the grid resolution of 6×80, whose curve is apparently differing from the experimental measurement, the results with

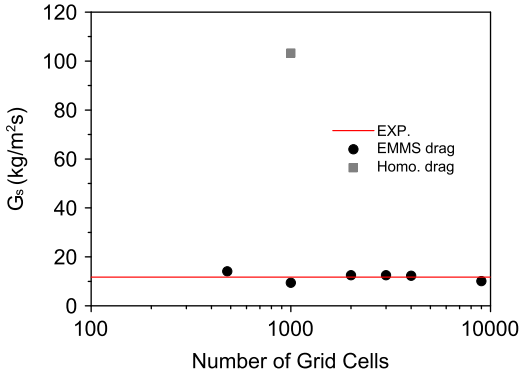

Fig. 2. Solids flux at the top exit of riser 1 with different grid number (calculated with EMMS and homogeneous drag force models, $D = 0.05$ m, H=2.79 m, $n_p = 100$, $e_w = 0.9$, the detailed grid information are listed in Table 1).

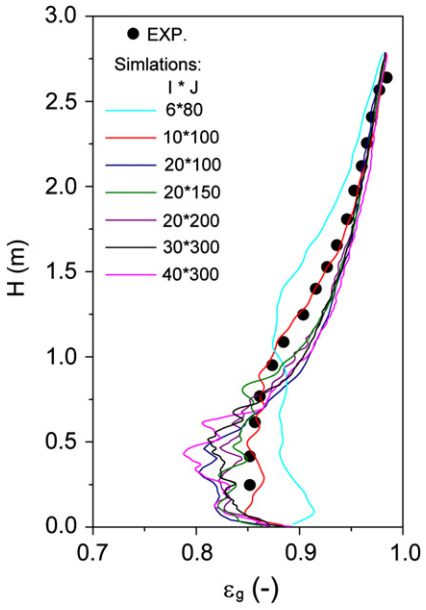

Fig. 3. Axial voidage distribution of riser 1 with different grid resolutions, I and J are the number of radial cells and vertically cells, respectively (calculated with EMMS and homogeneous drag force models, D=0.05 m, $H = 2.79$ m, $n_p = 100$, $e_w = 0.9$; sectional averaged voidage is used here and in the subsequent axial voidage distributions).

grid resolution higher than 10×100 are similar to each other and also very close to the experimental measurement. So, the grid resolution of 10×100 was used for riser 1 subsequently.

3.2. Verification of the MP-PIC method with EMMS drag

To verify the accuracy of the MP-PIC method with EMMS drag force model, the simulation results are compared with the experimental data.

3.2.1. Solid flux

Fig. 4a shows that, for riser 1 the solid flux calculated with the EMMS drag force model tends to be stable after about 5 s and then it fluctuates around an average value which is very close to the experimental measurement. The calculated solid flux with the homogeneous drag force model shows the same trend, except that its average value is much higher than the experimental measurement and the fluctuation value is also larger than that for the EMMS model. For riser 2, the calculated solid fluxes with

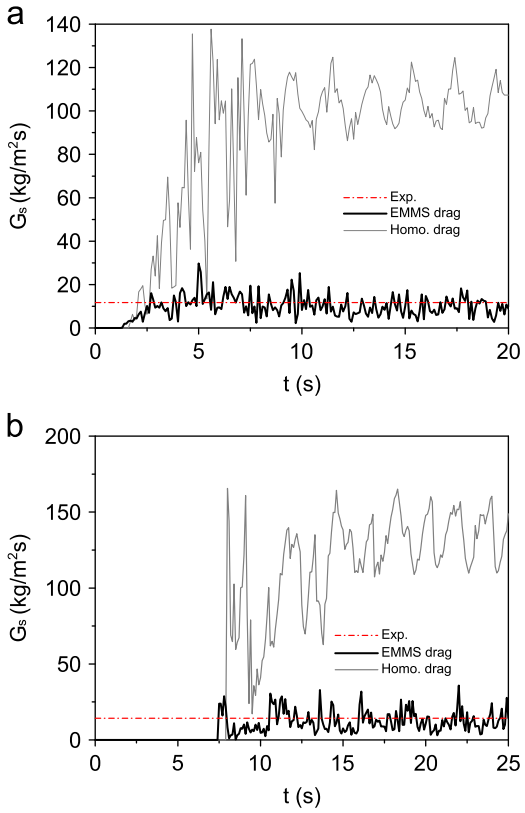

Fig. 4. Solids flux calculated with EMMS and Homo. drag force models at top exit, Homo. is short for homogeneous here and in the subsequent figs.: (a) riser 1, grid=10×100, $n_p = 100$, $e_w = 0.9$ and (b) riser 2, grid=40×225, $n_p = 500$, $e_w = 0.9$.

EMMS and homogeneous drag force models show the similar characteristics as those for riser 1, except that they become stable after about 10 s as shown in Fig. 4b.

3.2.2. Solid distribution in the whole field

Fig. 5 shows the voidage distribution of riser 1 at different instants. The data in Fig. 5a show that most of the solids reside in the bottom region of the riser while it is quite dilute in the top. And radially, the solid is also dense near the wall while dilute in the core which shows the so called "core-annular" structure. In addition, particles tend to aggregate locally to form heterogeneous meso-scale structures. Unlike the results calculated by the EMMS drag force model, the data in Fig. 5b which was calculated with homogeneous drag force model show quite different results. The solids are nearly uniformly distributed axially and it is much denser in the core than near the wall. The above trends can also be found in the particle type solid distribution as shown in Fig. 6 with color showing the particle velocity. Fig. 6a shows that particle velocity is high in the core and low near the wall in general. And in the core region, the velocity of the particles in aggregates is apparently lower than that of the particles in the dilute region. Fig. 6b which shows that the particle velocity calculated with homogeneous drag force model is nearly uniform all through the riser and the velocity range is quite narrow compared to Fig. 6a. Though not displayed here, riser 2 shows a very similar particle distribution as that of riser 1.

3.2.3. Axial voidage distribution

Fig. 7 compares the simulated axial voidage distributions with the experimental data. For both the risers, it can be found that, the simulated results with EMMS drag force model agree well with the experimental measurements showing a dilute top and

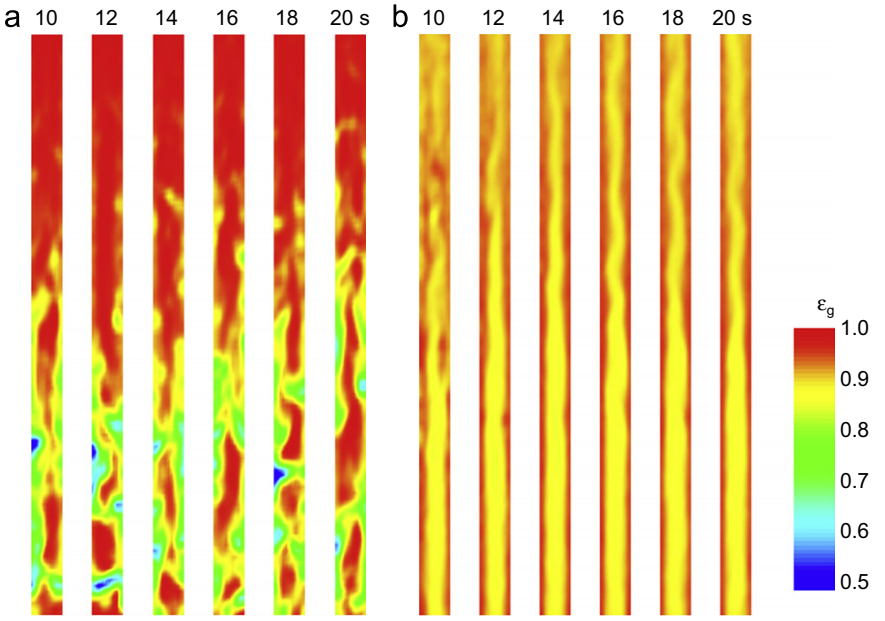

Fig. 5. Contour of voidage distribution for riser 1 at different instant (from 10 to 20 s, grid=10 × 100, $n_p = 100$, $e_w = 0.9$): (a) calculated with EMMS drag force model and (b) calculated with homogeneous drag force model.

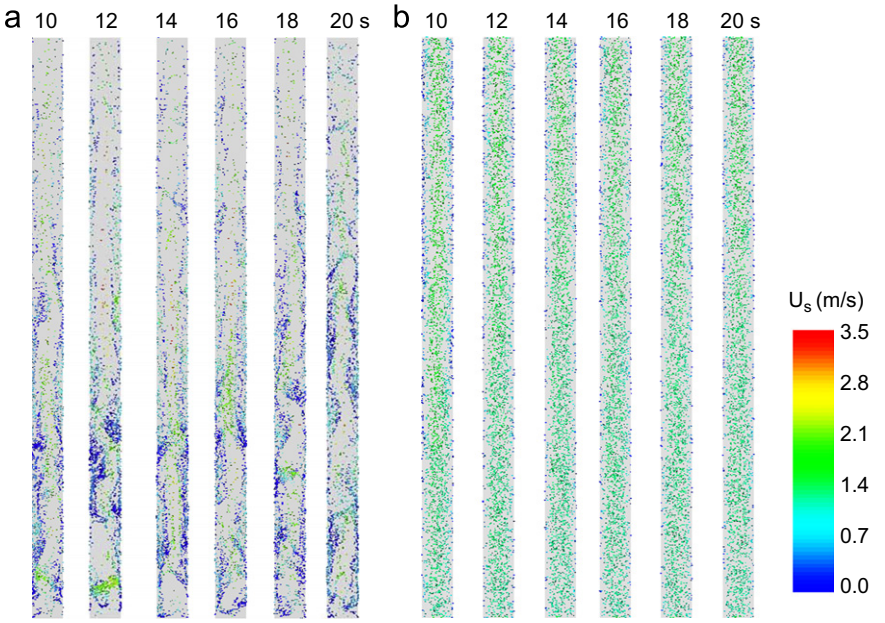

Fig. 6. Particle distribution for riser 1 at different instant (from 10 to 20 s, grid=10 × 100, $n_p = 100$, $e_w = 0.9$): (a) calculated with EMMS drag force model and (b) calculated with homogeneous drag force model.

dense bottom profiles, while the results predicted using homogeneous drag force model deviate much from the measurement, showing a nearly uniform distribution.

3.2.4. Radial distributions of solid volume fraction and solid velocity

Since, there is no experimental measurement for riser 2, only the data for riser 1 was analyzed. In Horio's experiments, a double-top optical fiber probe was used to measure local solid volume fraction and solid velocity (Horio et al., 1988). Cross correlation function to the signals of the two tops was computed to obtain the time lag, then the solid velocity. Figs. 8 and 9 show the radial solid volume fraction distributions at two heights. The data in Fig. 8 shows that, for the EMMS model, the simulated solid volume fraction is lower in the center than near the wall, which is very close to the experimental. However, for the homogeneous drag force model, the simulated solid volume fraction is high in the center but lower near the wall, which is right opposite to the measurement.

The data in Fig. 9 shows that, the solid velocities predicted using both EMMS model and homogeneous drag force model show higher velocity in the center than near the wall. In comparison, the prediction with EMMS model is much closer to the measured data, showing negative solid velocity near the wall due to solid back mixing. While the prediction with homogeneous drag model shows uniform distribution.

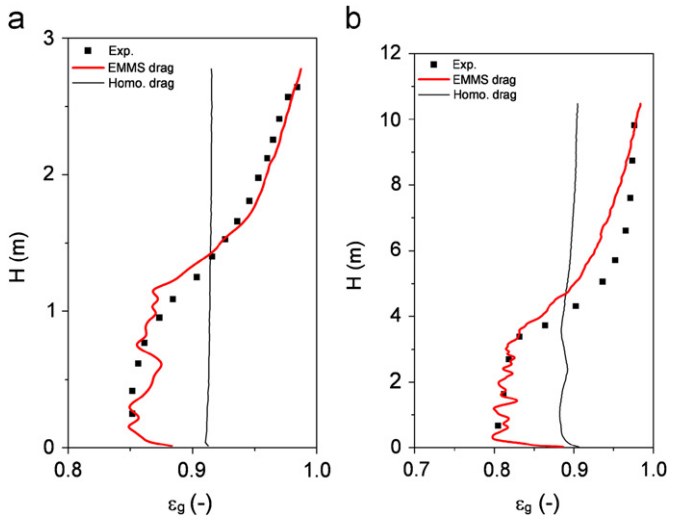

Fig. 7. Axial distribution of voidage for the risers: (a) riser 1, grid=10 × 100, $n_p = 100$, $e_w = 0.9$ and (b) riser 2, grid=40 × 225, $n_p = 500$, $e_w = 0.9$.

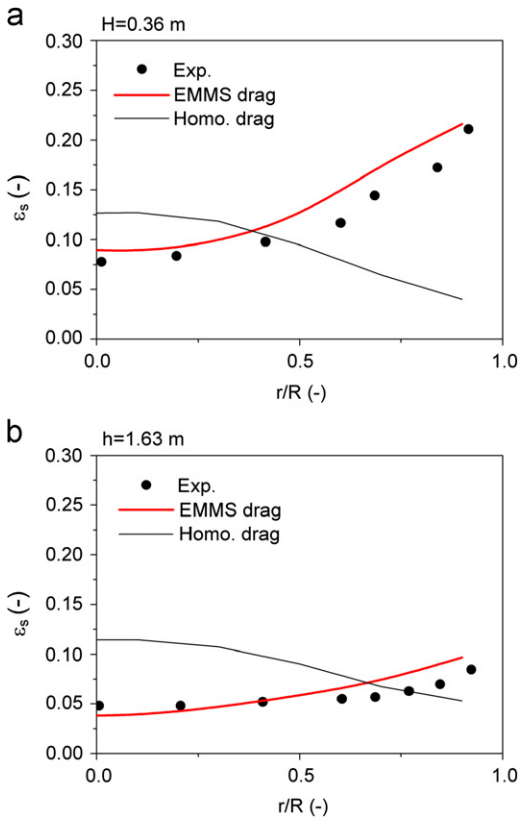

Fig. 8. Radial solid volume fraction distribution at two elevations for riser 1 (grid=10 × 100, $n_p = 100$, $e_w = 0.9$), here h is the distance of the surface away from inlet and it is the same in the subsequent figs.: (a) $h = 0.36$ m and (b) $h = 1.63$ m.

3.3. Parameter analysis

After verification of the model, particle–wall restitution coefficient, e_w, was first changed to investigate the effect of particle–wall condition on the simulation results. And then the very important parameter, number of particles per parcel, n_p, was also changed to investigate its effect on the simulation results and calculation efficiency. In this part, only riser 1 was simulated.

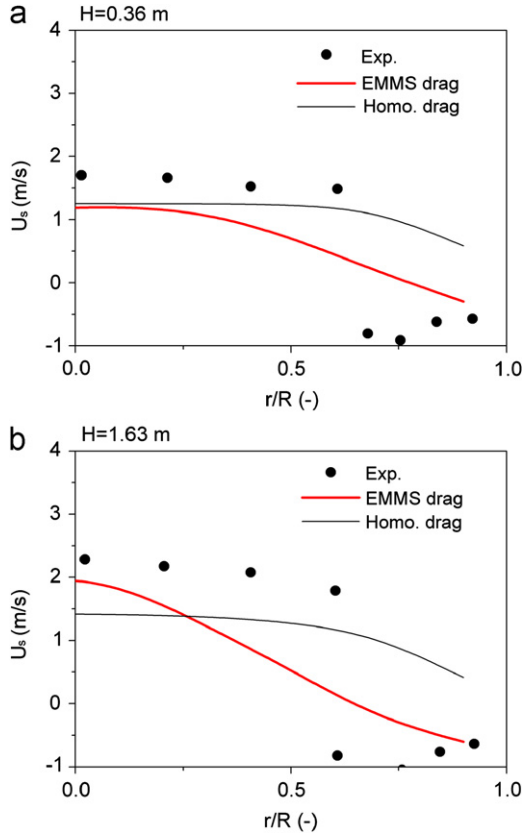

Fig. 9. Radial solid velocity distribution at two elevations for riser 1 (grid=10 × 100, n_p=100, $e_w = 0.9$): (a) $h = 0.36$ m and (b) $h = 1.63$ m.

Table 3
Predicted solids flux of riser 1 with different wall conditions.

Cases		Solids flux (kg/(m^2 s))	
Particle–wall restitution coefficient	Drag model	Sim	Exp
0.9	EMMS	10.4	11.7
	homogeneous	103.0	
0.99	EMMS	11.8	
	homogeneous	103.5	

3.3.1. Simulations with different wall restitution coefficient, e_w

In this section n_p=100 and two wall restitution coefficient (0.9 and 0.99) were used.

Table 3 compares the simulated solid flux with the experimental value. The data shows that when using EMMS drag model, the simulated solid flux with e_w=0.99 is closer to the measured value than that with e_w=0.9. However, both results are very similar to the measured value. The simulation result also changes little for the cases with homogeneous drag force model.

Fig. 10 shows that, when increasing e_w from 0.9 to 0.99, the predicted axial voidage distribution change little for both cases with different drag models. The same conclusion can be made with respect to the radial distributions of solid volume fraction and solid velocity as shown in Figs. 11 and 12.

3.3.2. Simulations with different number of particles per parcel, n_p

In this section e_w=0.9 and n_p =10–16,000 were used for all the cases.

Fig. 13 shows that when using EMMS drag force model, the simulated axial voidage distributions agree well with the experimental measurement under a wide range of n_p ($<$4000).

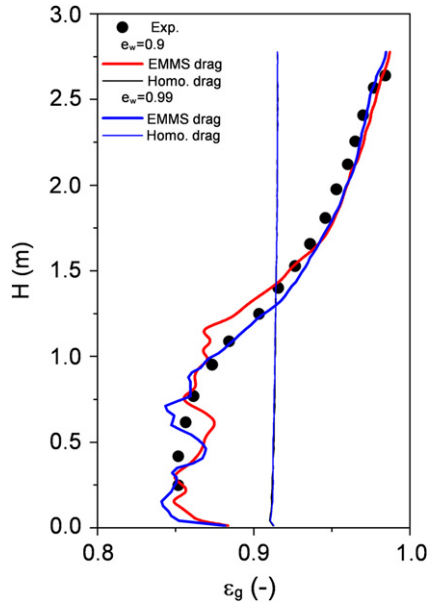

Fig. 10. Axial voidage distribution of riser 1 calculated with different wall conditions (D=0.05 m, H=2.79 m, e_w = 0.9, 0.99).

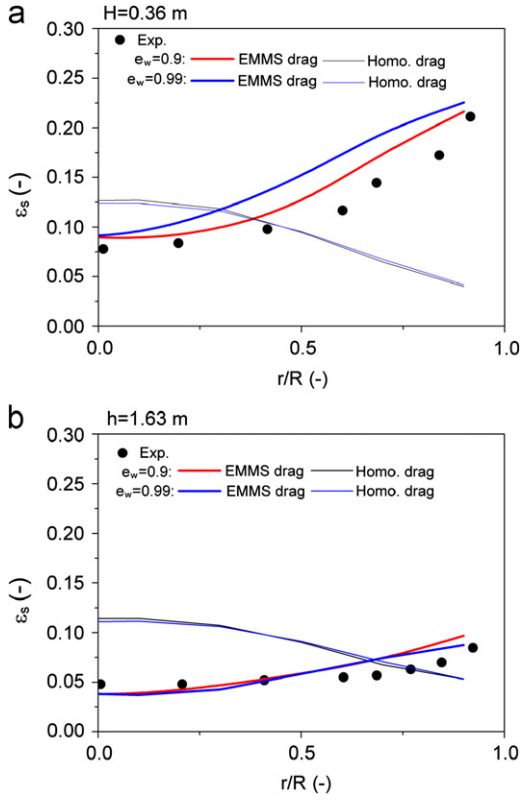

Fig. 11. Radial solid volume fraction distribution at two elevations of riser 1 calculated with different wall conditions (D=0.05 m, H=2.79 m, e_w = 0.9, 0.99): (a) h = 0.36 m and (b) h=1.63 m.

The axial voidage distribution deviates from the measurement data, only when n_p is larger than 4000 (8000 and 16,000, as shown by the dashpot lines in the figure), and the error increases with n_p. The figure also shows that, when n_p is larger than 4000, the profile decays downward, indicating that more and more particles tend to stay in the bottom. In this case, a wrong bubbling like fluidization phenomenon appears.

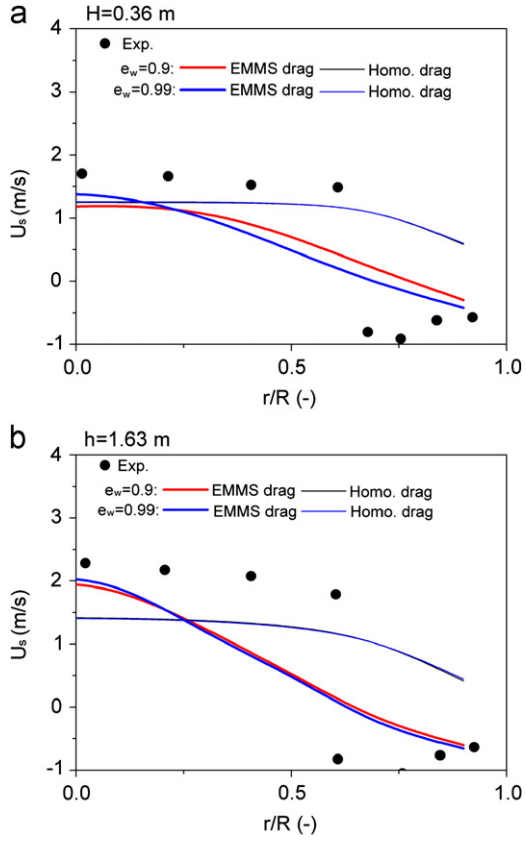

Fig. 12. Radial solid velocity distribution at two elevations of riser 1 calculated with different wall conditions (D=0.05 m, H = 2.79 m, e_w = 0.9, 0.99): (a) h = 0.36 m and (b) h=1.63 m.

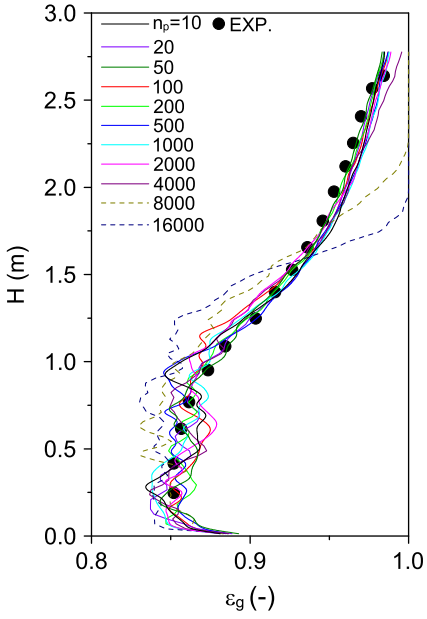

Fig. 13. Axial voidage distribution of riser 1 with different n_p (calculated with EMMS drag force model, D=0.05 m, H=2.79 m, n_p = 10–16,000).

Figs. 14 and 15 show the relationship between solid flux, simulation time and the number of particles per parcel. The normalized number of particles per parcel which is expressed as the ratio between the total volume of particles in a parcel and the computational cell volume is also presented on the top of the figures.

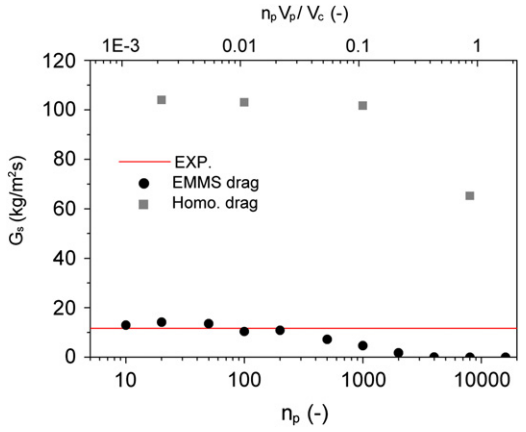

Fig. 14. Solids flux at the top exit of riser 1 with different n_p, the bottom coordinate axis is the absolute value of n_p and the top coordinate axis is the normalized value (calculated with EMMS and homogeneous drag force models, D=0.05 m, H=2.79 m).

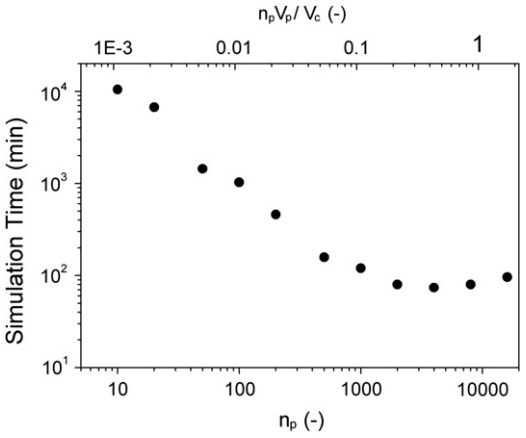

Fig. 15. Simulation time for riser 1 with different n_p, the bottom coordinate axis is the absolute value of n_p and the top coordinate axis is the normalized value (calculated with EMMS drag force model, D=0.05 m, H=2.79 m,).

Fig. 14 shows that, when using EMMS drag force model, the calculated solid flux is almost zero if n_p is larger than 8000, which corresponds to the wrong predictions shown in Fig. 13. With the decrease of n_p, the solid flux increases gradually until n_p is less than 500, when the solid flux becomes stable and its value agrees very well with the experimental measurement. When using homogeneous drag force model, the calculated solid flux is about an order of magnitude higher than the experimental value. For these cases the solid flux becomes stable when n_p is less than 1000 and the solid flux also decreases when n_p is larger than 1000.

Fig. 15 shows that, the elapsed simulation time tends to be stable after $n_p > 1000$; while it increases exponentially with decreasing n_p when $n_p < 1000$. This implies that, it is the fluid calculation that contributes most to the calculation when $n_p > 1000$. While for $n_p < 1000$, the particles calculation is dominant. For this sake, parallel computing with GPU or CPU may greatly improve the calculation efficiency(Xiong et al., 2010).

4. Conclusion and prospects

As the first step to realize rapid simulation of fluidizations, the EMMS drag force based MP-PIC method was implemented, and it was successfully used in the simulations of two CFB riser flows. Calculation results show that, EMMS drag force model based simulation can not only predict the macroscopic bottom dense and top dilute axial solid distribution as well as the so called core-annular radial distribution, but it can also predict the meso-scale local particle aggregative. A remarkably high accuracy was also obtained by comparing the calculated solid flux and solid distribution data with the experimental measurements and the predicted results with the traditional homogeneous drag force model. Parameter analysis shows that:

(1) The particle–wall restitution coefficient has very limited effect on the axial voidage distribution and radial distributions of solid volume fraction and solid velocity.
(2) There exists a critical value for n_p, below which, the stable solid flux can be achieved, which is also very close to the experimental measurement.
(3) There exists another critical value for n_p, below which, the elapsed simulation time increases with the increasing of n_p.

This study implies that EMMS drag force model based MP-PIC method can be used as the basis of rapid simulation while it is far from fulfillment. Further efforts are needed such as to facilitate the present program with the capacity of parallel computing based on CPU and GPU platforms and much more, the capacity of managing complex geometry is also very necessary.

Notation

a, b, c	EMMS drag force model parameter
d_p	particle diameter (m)
e_w	restitution coefficient for particle–wall collision
H_D	heterogeneity index
n_p	number of particles per parcel
n_T	parcel number in fluid cell
p	gas pressure (Pa)
p_s	particle pressure (Pa)
P_s^*	particle pressure model parameter (Pa)
$\vec{u}_g$	gas phase velocity at cell center (m/s)
$\vec{U}_g(\vec{x}_p)$	gas velocity at parcel location (m/s)
$\vec{U}_p$	parcel velocity (m/s)
$\vec{U}_p^{(0)}$	parcel velocity before collision with wall (m/s)
V_c	fluid cell volume (m^3)
V_p	particle volume (m^3)
$\vec{x}_p$	parcel location (m)
$\bar{\bar{S}}_g$	gas phase strain tensor (m^{-1})
Re_p	particle Reynolds number

Greek letters

α	particle pressure model parameter
β_p	drag force coefficient (kg/m^3 s)
ε_g	gas volume fraction
ε_s	particle volume fraction
$\varepsilon_{s,\max}$	solid volume fraction at close pack
ρ_g	gas density (kg/m^3)
$\bar{\bar{\tau}}_g$	gas phase stress tensor (Pa)
μ_g	gas viscosity (Pa s)

Subscripts

g	gas phase
s	particle phase

Acknowledgment

This work was financially supported by the National Natural Science Foundation of China (Nos. 21106159 and 20821092, 21176240) and MOST (Nos. 2011DFA61360 and 2012CB215003) and CAS (Nos. KGCXZ-YW-222 and XDA07080404).

References

Andrews, M.J., O'Rourke, P.J., 1996. The multiphase particle-in-cell (MP-PIC) method for dense particulate flows. Int. J. Multiphase Flow 22 (2), 379–402.

Benyahia, S., 2011. Analysis of model parameters affecting the pressure profile in a circulating fluidized bed. AIChE J. 58, 427–439.

Benyahia, S., Galvin, J.E., 2010. Estimation of numerical errors related to some basic assumptions in discrete particle methods. Ind. Eng. Chem. Res. 49, 10588–10605.

Benyahia, S., Sundaresan, S., 2011. Do we need sub-grid scale corrections for both continuum and discrete gas-particles flow models? Powder Technol. 220, 2–6.

Breault, R.W., 2012. An analysis of clustering flows in a CFB riser. Powder Technol. 220 (0), 79–87.

Chen, F., Ge, W., Guo, L., He, X., Li, B., Li, J., Li, X., Wang, X., Yuan, X., 2009. Multi-scale HPC system for multi-scale discrete simulation—development and application of a supercomputer with 1 Petaflops peak performance in single precision. Particuology 7 (4), 332–335.

Chu, K.W., Yu, A.B., 2008. Numerical simulation of complex particle-fluid flows. Powder Technol. 179 (3), 104–114.

Deen, N.G., Van Sint Annaland, M., Van der Hoef, M.A., Kuipers, J.A.M., 2007. Review of discrete particle modeling of fluidized beds. Chem. Eng. Sci. 62 (1-2), 28–44.

Ergun, S., 1952. Fluid flow through packed columns. Chem. Eng. Prog. 48 (1), 89–94.

Galimov, A.Y., Drew, D.A., Lahey, J.R.T., Moraga, F.J., 2005. The analysis of interfacial waves. Nucl. Eng. Des. 235 (10-12), 1283–1292.

Ge, W., Wang, W., Yang, N., Li, J., Kwauk, M., Chen, F., Chen, J., Fang, X., Guo, L., He, X., Liu, X., Liu, Y., Lu, B., Wang, J., Wang, J., Wang, L., Wang, X., Xiong, Q., Xu, M., Deng, L., Han, Y., Hou, C., Hua, L., Huang, W., Li, B., Li, C., Li, F., Ren, Y., Xu, J., Zhang, N., Zhang, Y., Zhou, G., Zhou, G., 2011. Meso-scale oriented simulation towards virtual process engineering (VPE)—the EMMS Paradigm. Chem. Eng. Sci. 66 (19), 4426–4458.

Gidaspow, D., 1994. Multiphase Flow and Fluidization: Continuum and Kinetic Theory Descriptions. Academic Press, Boston.

Horio, M., Morishita, K., Tachibana, O., Murata, N., 1988. Solid Distribution and Movement in Circulating Fluidized Beds. Circulating Fluidized Bed Technology II. Pergamon.

Ishii, M., 1975. Thermo-fluid Dynamic Theory of Two-phase Flow. Eyrolles Press, Paris.

Jiradilok, V., Gidaspow, D., Damronglerd, S., Koves, W.J., Mostofi, R., 2006. Kinetic theory based CFD simulation of turbulent fluidization of FCC particles in a riser. Chem. Eng. Sci. 61 (17), 5544–5559.

Kuwagi, K., Takeda, H., Horio, M., 2004. The similar particle assembly (SPA) model: an approach to large-scale discrete element (DEM) simulation. In: International Conference on Fluidization Engineering XI, Ischia, Naples, pp. 243–250.

Li, F., 2009. Investigations on the Turbulent Gas–Solid Two-phase Interactions in Fluidized Desulfurization Process. Doctor Dissertation. Tsinghua University, Beijing.

Li, J., Kwauk, M., 1994. Particle-fluid Two-phase Flow, the Energy-minimization Multi-scale Method. Metallurgical Industry Press, Beijing.

Liu, X., Liu, Y., Xu, X., Song, S., 2006. Studing on cluster behavior in dense gas-particle two-phase flow by using DEM model. J. Eng. Thermophys. 27 (3), 519–522.

Lu, B., 2009. EMMS-based Meso-scale Model and Its Application in Simulating Gas–Solid Two-Phase Flows. Doctor Dissertation. Chinese Academy of Science, Beijing.

Lu, B., Wang, W., Li, J., 2011. Eulerian simulation of gas–solid flows with particles of Geldart groups A, B and D using EMMS-based meso-scale model. Chem. Eng. Sci. 66 (20), 4624–4635.

Mokhtar, M.A., Kuwagi, K., Takami, T., Hirano, H., Horio, M., 2011. Validation of the similar particle assembly (SPA) model for the fluidization of Geldart's group A and D particles. AIChE J., 87–98.

Neri, A., Gidaspow, D., 2000. Riser hydrodynamics, simulation using kinetic theory. AIChE J. 46 (1), 52–67.

Nikolopoulos, A., Atsonios, K., Nikolopoulos, N., Grammelis, P., Kakaras, E., 2010. An advanced EMMS scheme for the prediction of drag coefficient under a 1.2 MWth CFBC isothermal flow—Part II: numerical implementation. Chem. Eng. Sci. 65 (13), 4089–4099.

Patankar, N.A., Joseph, D.D., 2001. Modeling and numerical simulation of particulate flows by the Eulerian–Lagrangian approach. Int. J. Multiphase Flow 27 (10), 1659–1684.

Pirker, S., Kahrimanovic, D., Kloss, C., Popoff, B., Braun, M., 2010. Simulating coarse particle conveying by a set of Eulerian, Lagrangian and hybrid particle models. Powder Technol. 204 (2-3), 203–213.

Qi, H., Li, F., Xi, B., You, C., 2007. Modeling of drag with the Eulerian approach and EMMS theory for heterogeneous dense gas–solid two-phase flow. Chem. Eng. Sci. 62 (6), 1670–1681.

Snider, D.M., 2001. An Incompressible three-dimensional multiphase particle-in-cell model for dense particle flows. J. Comput. Phys. 170 (2), 523–549.

Syamlal, M., Rogers, W., O'Brien, T.J., 1993. MFIX Documentation Theory Guide. Morgantown Energy Technology Center, Morgantown.

Tsuji, Y., Kawaguchi, T., Tanaka, T., 1993. Discrete particle simulation of two-dimensional fluidized bed. Powder Technol. 77 (1), 79–87.

Tsuji, Y., Tanaka, T., Ishida, T., 1992. Lagrangian numerical simulation of plug flow of cohesionless particles in a horizontal pipe. Powder Technol. 71 (3), 239–250.

Wang, J., Ge, W., Li, J., 2008a. Eulerian simulation of heterogeneous gas–solid flows in CFB risers: EMMS-based sub-grid scale model with a revised cluster description. Chem. Eng. Sci. 63 (6), 1553–1571.

Wang, W., Li, J., 2007. Simulation of gas–solid two-phase flow by a multi-scale CFD approach—extension of the EMMS model to the sub-grid level. Chem. Eng. Sci. 62 (1-2), 208–231.

Wang, W., Lu, B., Dong, W., Li, J., 2008b. Multi-scale CFD simulation of operating diagram for gas–solid risers. Can. J. Chem. Eng. 86, 448–457.

Wen, C.Y., Yu, Y.H., 1966. Mechanics of fluidization. AIChE Symp. Ser. 62, 100–111.

Xiong, Q., Li, B., Chen, F., Ma, J., Ge, W., Li, J., 2010. Direct numerical simulation of sub-grid structures in gas–solid flow—GPU implementation of macro-scale pseudo-particle modeling. Chem. Eng. Sci. 65 (19), 5356–5365.

Yang, N., Wang, W., Ge, W., Li, J., 2003. CFD simulation of concurrent-up gas–solid flow in circulating fluidized beds with structure-dependent drag coefficient. Chem. Eng. J. 96 (1-3), 71–80.

Zhang, N., Lu, B., Wang, W., Li, J., 2008. Virtual experimentation through 3D full-loop simulation of a circulating fluidized bed. Particuology 6 (6), 529–539.

Zhang, N., Lu, B., Wang, W., Li, J., 2010. 3D CFD simulation of hydrodynamics of a 150 MWe circulating fluidized bed boiler. Chem. Eng. J. 162 (2), 821–828.